Mem. Natl Inst. Polar Res., Spec. Issue, 52, 55–67, 1998

NEUTRAL ATMOSPHERE DYNAMICS IN THE *E*- AND *F*-REGIONS FROM FABRY-PEROT DOPPLER IMAGING OBSERVATIONS

Minoru KUBOTA[1], Shoichi OKANO[2] and Hiroshi FUKUNISHI[3]

[1] *Communications Research Laboratory, Nukui-Kitamachi 4-chome, Koganei-shi, Tokyo 184-8795*
[2] *National Institute of Poler Research, Kaga 1-chome, Itabashi-ku, Tokyo 173-8515*
[3] *Department of Geophysics, Faculty of Science, Tohoku University, Aoba-ku, Sendai 980-8578*

Abstract: In order to investigate a response of the thermospheric neutral winds to the auroral activity, we developed a Fabry-Perot Doppler Imaging System (FPDIS) which measures Doppler shifts and widths of aurora and/or airglow emission lines of OI 557.7 nm and OI 630.0 nm over a wide field of view (165°) to obtain two-dimensional patterns of winds and temperatures in the *E*- and *F*-regions. We carried out the FPDIS observations at Syowa Station (69.00°S, 39.58°E), Antarctica over 57 nights covering the various auroral conditions in 1994. In this paper, we discuss the following results obtained from our observations: (1) We found that nighttime variations in the thermospheric neutral winds depend on geomagnetic activity. Magnetically southward winds during geomagnetically active periods were stronger than during quiet periods, and the difference in the wind velocities was largest around midnight. This difference is supposed to be associated with auroral energy injection and the relative location between the auroral oval and Syowa Station. (2) Periodic enhancements in meridional winds, which were classified into middle-scale atmospheric gravity waves (AGWs), were observed on the night of 3–4 June 1994 during geomagnetically active periods. These wind enhancements appeared to be generated in the auroral oval which remained at a few hundred kilometers north of Syowa Station.

1. Introduction

Fabry-Perot interferometers have been used for many years to measure winds and temperatures in the upper thermosphere from line-of-sight Doppler shifts and widths of the OI 630.0 nm emission line, for example ARMSTRONG (1969), HAYS and ROBLE (1971), HERNANDEZ and ROBLE (1976), SIPLER and BIONDI (1979), JACKA *et al.* (1979), HAYS *et al.* (1979), BURNSIDE *et al.* (1981), SICA *et al.* (1989), HERNANDEZ *et al.* (1990) and others. A classical Fabry-Perot interferometer has a photomultiplier at the center of a pinhole on the image plane of interference fringes by a Fabry-Perot etalon. Etalon scanning by changing the pressure within the etalon cavity or by changing the etalon's plate separation has widely been used as a mean of producing an emission line spectrum. MERIWETHER *et al.* (1988) reported on ground-based measurements of neutral winds from the central polar cap at Thule under the solar minimum conditions for the first

time. Winds in the geomagnetic polar cap had a fundamentally diurnal antisunward character, in accord with model predictions, with typical speeds of ~200 m/s. A large variability in both the magnitude and direction of winds was observed in the neutral flow, including evidence for curvature within the ~400 km diameter field of view. They concluded that even at solar minimum, the forcing by the polar cap convection pattern remains strong enough to give a significant influence on the geometry of the polar cap neutral wind field.

Recently, some significant improvements in the étendue of the Fabry-Perot interferometer have been made by using imaging photon detectors to record the entire Fabry-Perot fringe in the image plane. REES and GREENAWAY (1983) discussed alternative means of obtaining a higher étendue from an etalon, and described the concept of a Doppler imaging system (DIS) which would have a multiplex advantage of at least 100 times that of the classical interferometer. The DIS is also capable of deducing a two-dimensional velocity field of a suitable line-emitting areal source by an independent measuring of the Doppler shift at a large number of points within the field of view. REES *et al.* (1984) presented the results of initial observations on the auroral thermosphere at Kiruna, using a prototype DIS which had an 80 field of view. BATTEN *et al.* (1988) and BATTEN and REES (1990) presented new data from an upgraded UCL-DIS, which had been developed specifically to detect small-scale thermospheric wind structures with short time scales. The data confirmed that the thermosphere was very dynamic, even with a high degree of variability on small spatial (50 km) and temporal (10 min) scales. Typical eddy scale sizes of 100–300 km were observed near midnight.

A prototype of the Fabry-Perot Doppler Imaging System (FPDIS) was developed by the Tohoku University optical group to observe two-dimensional structure of the thermospheric wind velocities and temperatures. The FPDIS is able to measure Doppler shifts and widths of aurora emission lines of atomic oxygen OI 557.7 nm and OI 630.0 nm over a 165° field of view (NAKAJIMA, 1993; NAKAJIMA *et al.*, 1995). This system was used for observing the thermospheric wind velocities and temperatures at Syowa Station, Antarctica during the whole austral winter in 1990, and it detected large variations in the neutral thermospheric temperatures and wind velocities associated with auroral break up events.

In order to investigate the response of the thermospheric neutral winds to auroral activity, we made overall improvements to the prototype FPDIS in 1993. The most important characteristic of the new FPDIS was high temporal and spatial resolution in the thermospheric wind measurements. The maximum time resolutions for FPDIS measurement were 1 min and 3 min for OI 557.7 nm and OI 630.0 nm emissions, respectively, while typical spatial resolutions for these emissions were about 50 km and 100 km. We installed the new FPDIS at Syowa Station (69.00°S, 39.58°E, 66°INV, L ~6.1) in February 1994, and observed the thermospheric neutral winds over 57 nights covering various auroral conditions in the austral winter of 1994. Since Syowa Station is located just within the auroral zone, the site is quite suitable to observe variations in the thermospheric winds directly associated with auroral disturbances. In addition, there are many kinds of facilities at Syowa Station to observe auroral, magnetic and ionospheric disturbances, namely an SIT all-sky camera for auroral observations, fluxgate and search coil magnetometers for geomagnetic field observations, an ionosonde

and a multi-beam riometer for ionosphere observations.

2. Fabry-Perot Doppler Imaging System

The FPDIS consists of optical lenses, a Fabry-Perot etalon, interference filters, a two-dimensional photon detector, and an image data processing system. All-sky images (field of view = 165°), focused by an objective fish-eye lens, are reduced by a relay lens system and then collimated to nearly parallel beams so as to cause interference in the Fabry-Perot etalon. The etalon used in the FPDIS is a piezo-electrically tuned and servo-stabilized etalon (Model ET116, Queensgate Instruments, Ltd.). Etalon fringes are focused on the photocathode of a proximity focused photon counting imager (PFPCI) with a focusing lens. The PFPCI, which is cooled down to −15°C, is a highly sensitive, two-dimensional photon detector (Model V5102UX, Hamamatsu Photonics Corp.). Two interference filters, which are placed between the focusing lens and the PFPCI, are used to select the wavelengths of auroral emissions of OI 630.0 nm and OI 557.7 nm. The output image on the fluorescent screen of the PFPCI is reduced and finally focused on a CCD camera. Composite video signals from the CCD camera are transferred to digital images composed of 512 (H) × 480 (V) pixels, and they are discriminated and integrated by the image data processor, where the threshold is adjusted to allow the majority of photoelectron pulses to pass and block the majority of other pulses caused by noise. Finally, the fringe image data are recorded on a 5″ magnetic optical disk (MO disk). To check instrumental errors arising from thermal drifts in etalon parameters, the FPDIS is equipped with a stabilized He-Ne calibration laser. The beam of the He-Ne laser is diffused and enters the optical path of the FPDIS through a beam splitter.

3. Observations and Data Analysis

3.1. FPDIS observations at Syowa Station

We obtained FPDIS data over 57 nights from March to September 1994 at Syowa Station, Antarctica. This data set covered various auroral conditions.

Figure 1 is a conceptual sketch showing the configuration for FPDIS observation. In the image plane, there are two complete etalon fringes which are projected onto the full field of view of 165° in the sky. Thus, the fringes of an auroral emission of OI 630.0 nm with a peak emission altitude of ~240 km cover a region of approximately 700 km in diameter, while the fringes of an auroral emission of OI 557.7 nm with a peak emission altitude of ~105 km cover a region of approximately 360 km in diameter.

All operations of the FPDIS were automatically executed by instructions from a personal computer. For example, the selection of the OI 630.0 nm and OI 557.7 nm emission lines were automatically selected by rotating the filter wheel. The personal computer also controlled the time sequences for FPDIS operation. Fringe image data read out from the CCD were integrated by the image processor. The integration time was usually 150–240 s for OI 630.0 nm emission and 18–30 s for OI 557.7 nm emission. It took 30 s to save each piece of image data on a MO disk. If necessary, the filter wheel was rotated during this time interval. During the observation sequence, the cycles for

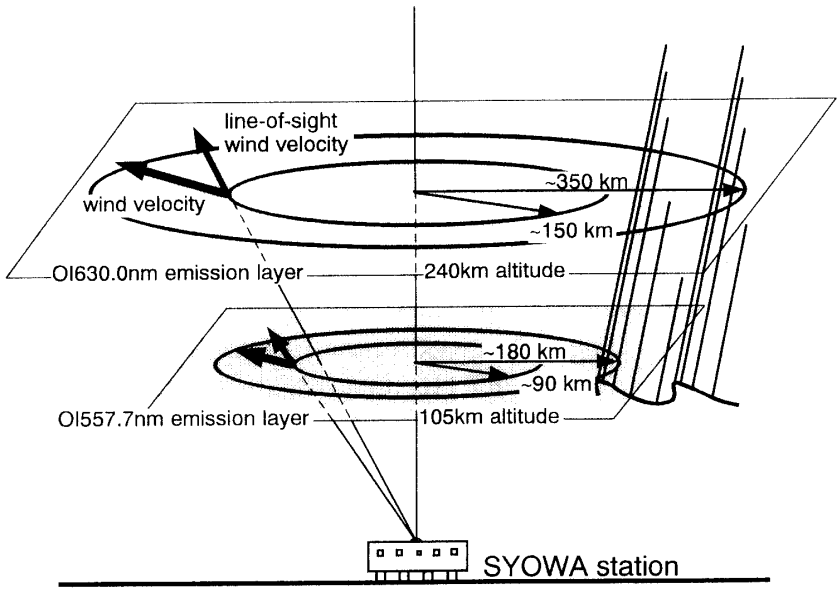

Fig. 1. Configuration of observations with the FPDIS.

three successive fringe images, one OI 630.0 nm fringe image and two OI 557.7 nm fringe images, were repeated. Fringe images of the He-Ne calibration laser beam were also taken every hour to check thermal drifts of etalon parameters.

3.2. Data analysis

Fringe images obtained by the FPDIS were sliced in azimuthal directions every 15 degrees, and converted to 24 sliced profiles. Each sliced fringe profile was fitted with the Gaussian function using a non-linear least squares method, and peak positions were determined. We obtained the Doppler shifts of auroral emission lines which indicated line-of-sight (LOS) wind velocities in the thermosphere from the difference between these peak positions and 'windless fringe' peak positions. The LOS wind velocities were calculated at a total of 48 points with 24 each for inner and outer fringes.

The windless fringe, which is necessary to estimate the Doppler wind velocity, was obtained by the following procedure. Fringe images of aurora obtained during weak auroral activity were selected first. We can assume that there is no vertical wind during such periods. Then the fringe images over a few hours were superimposed to improve the signal-to-noise ratio. The superimposed fringe image was divided into 24 sectors with 15 degree azimuthal separations, and each fringe radius was determined. The average of the fringe radii in the 24 azimuthal directions was adopted as the windless fringe radius, since wind divergence or convergence along a closed path for each fringe was considered to be very small when there was no vertical wind.

Because random errors in wind velocities rapidly increase as peak counts drop to less than 150, we did not use FPDIS data when peak counts were less than 150. In this case, random errors in wind velocities derived from OI 630.0 nm emission fringes were estimated to be less than 25 m/s for the inner fringe, and 35 m/s for the outer fringe. With OI 557.7 nm emission, errors in derived wind velocities were thought to decrease, since the peak counts of OI 557.7 nm emission fringes were usually larger than those of

OI630.0 nm emission fringes, and the kinetic temperature of the OI557.7 nm emission layer at ~100 km is lower than that of the OI630.0 nm emission layer at ~250 km.

Non-uniformity of auroral luminosity also affects wind velocity estimations, because it causes shifts in fringe peak positions. The error in wind velocity increases as the gradient of source emission intensity increases, and sometimes it may be over 50 m/s (KUBOTA, 1996). However, it is difficult to estimate an exact value for non-uniformity in auroral luminosity, since monochromatic imaging observations were not carried out simultaneously. It is likely that weak auroras do not cause large errors. However, it is necessary to consider the effect of non-uniform luminosity for bright and stable auroras.

4. Observational Results

4.1. F-region wind patterns on quiet and disturbed days

FPDIS data set obtained in the two periods of 10–13 July 1994 and 1–4 June 1994 was analyzed in detail to investigate the thermospheric wind patterns during quiet and disturbed periods. Figure 2 shows variations of K_p indices and K indices at Syowa Station during these periods. During the first period, geomagnetic activity was very low with K_p values ranging from 0 to 2$_-$, and auroral activity was also very low. The values of F10.7 solar flux ranged from 84.1 to 88.9. During the second period, geomagnetic activity was high with K_p values ranging from 3$_-$ to 5, and active auroras were frequently observed. The values of F10.7 solar flux ranged from 69.5 to 70.3.

To estimate large scale variations in meridional and zonal winds in the thermosphere, the LOS wind velocities we obtained were processed as follows. First, the LOS wind velocities were transformed into horizontal wind velocities assuming that there was no vertical wind. Next, these horizontal wind velocities were averaged in the sectors shown in Fig. 3 to reduce fluctuations due to small scale wind variations. Here, we

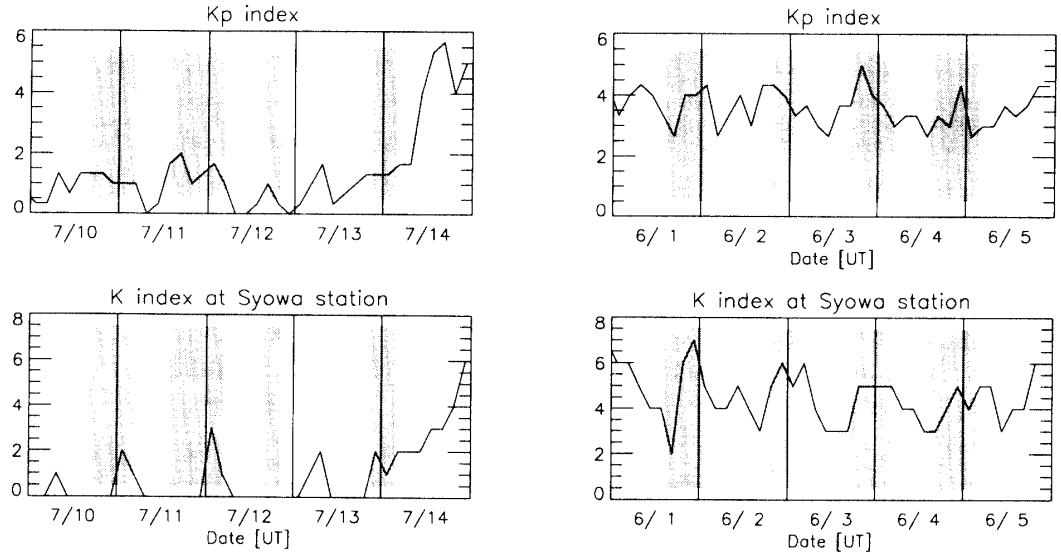

Fig. 2. K_p indices and K indices at Syowa Station during the two periods from 1–5 June 1994 and 10–14 July 1994. Hatched areas represent when FPDIS observations were done.

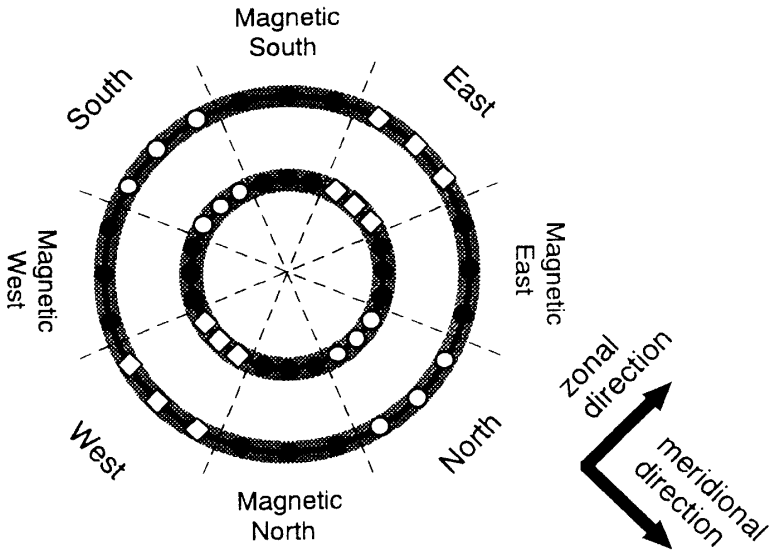

Fig. 3. Geometry to derive the averaged meridional and zonal wind velocities from the OI 630.0 nm fringe image data. The average values of horizontal wind velocities at the positions indicated by '○' or '◇' were adopted as average meridional or zonal wind velocities, respectively. Note that geomagnetic coordinates are rotated by 42 degrees against geographical coordinates at Syowa Station.

must note that the geomagnetic coordinates are rotated by 42 degrees against the geographical coordinates at Syowa Station.

Figure 4 shows the variations in meridional (solid lines) and zonal (broken lines) winds observed at OI630.0 nm emission height. This figure shows the wind velocity variations for all four nights from 10 July 1994 to 13 July 1994. The relation between geomagnetic local time (MLT) at Syowa Station and UT is given by MLT $\simeq$ UT. To show a comparison of these observational results with NCAR-TIGCM simulation results, the calculated winds (thick lines) at an altitude of 240 km (*F*-region) were superimposed on the meridional and zonal wind variations. It is apparent from Fig. 4 that wind variations obtained by the TIGCM simulation agree with the observed meridional and zonal winds in the *F*-region. The TIGCM was run for winter solstice conditions in the southern hemisphere and F10.7 = 90 by R.G. ROBLE of the National Center of Atmospheric Research (ROBLE and RIDLEY, 1987). When geomagnetic activity is low, the thermospheric wind is mainly driven by both the pressure gradient force along the 14–02 LT plane and convective ion drag force. Therefore, the wind patterns we obtained are consistent with the TIGCM model simulations during the geomagnetic quiet time.

However, the variations in meridional and zonal winds during geomagnetically disturbed periods were quite different from those during geomagnetically quiet periods. Figure 5 shows the wind velocity variations over all four nights from 1 June 1994 to 4 June 1994. The *F*-region winds during active periods (Fig. 5) are more southward and eastward compared to winds during quiet periods (Fig. 4). To further investigate the difference in wind patterns on quiet and disturbed days, we plotted *F*-region neutral

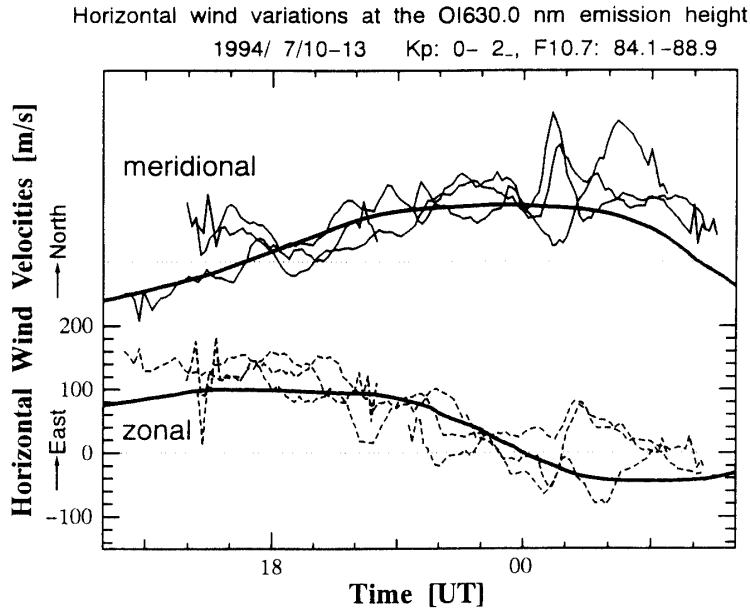

Fig. 4. Variations in meridional (solid lines) and zonal (broken lines) winds derived from Doppler imaging data of OI630.0 nm emission. Wind velocity data for the 4 nights from 10 July 1994 to 13 July 1994 are shown together. On these nights, wind velocities were derived every ~5 min, but they were smoothed by the boxcar average of a 5-point width. Calculated winds (thick lines) were superimposed on the meridional and zonal wind variations.

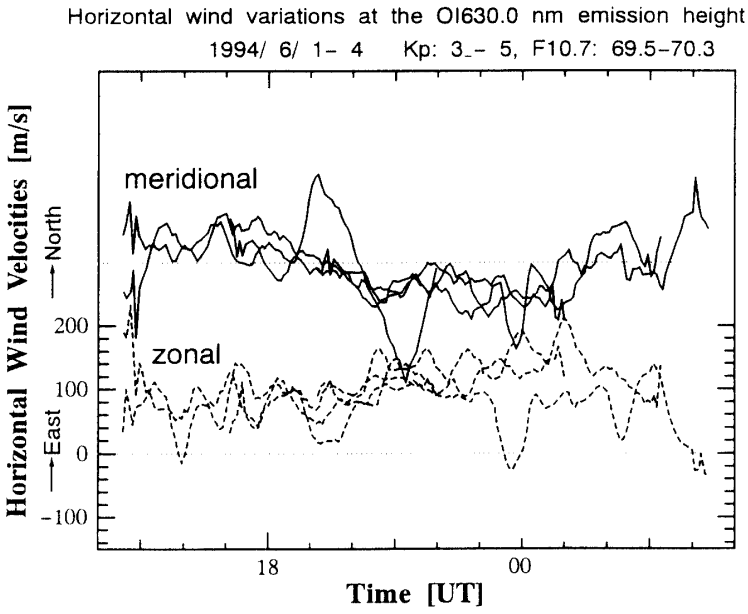

Fig. 5. Variations in meridional (solid lines) and zonal (broken lines) winds derived from Doppler imaging data of OI630.0 nm emission for the 4 nights from 1 June 1994 to 4 June 1994.

winds using geomagnetic coordinates rotated ~45 degrees against geographical coordinates (not shown). From these, we found that nighttime variations in magnetic east-west winds were roughly the same on disturbed days and quiet days, but magnetic north-south winds were apparently more southward (poleward) on disturbed days than on quiet days. Around midnight, the difference in wind velocities became greatest and exceeded 100–200 m/s.

We think that this difference is associated with auroral energy injection and the relative location between the auroral oval and Syowa Station. The auroral oval expands with increasing geomagnetic activity. FELDSTEIN and STARKOV (1967) determined the width and location of the auroral oval using observational data obtained with a broad network of all-sky cameras. Based on their results, Syowa Station (-66.23° geomagnetic latitude) is usually located equatorward of the mean auroral oval at night on quiet days. However, during moderately active conditions, Syowa Station appears to be located mostly within the oval at night. Under significantly active conditions, it is possible that Syowa enters the polar cap region around magnetic midnight. Further, auroral all-sky images obtained by the SIT camera at Syowa Station also indicate that it was located equatorward of the mean auroral oval at night from 10–13 July 1994, and entered the polar cap region around magnetic midnight from 1–4 June 1994. In the auroral oval, heating of the neutral atmosphere occurs through Joule heating and auroral particle precipitation, producing pressure gradients (FOSTER *et al.*, 1983; REES *et al.*, 1983). Such pressure gradients can drive a divergent wind field, such as poleward winds on the higher latitude side of the auroral oval, and equatorward winds on the lower latitude side of it. These winds could be increased during disturbed periods and affect the neutral circulation pattern of the thermosphere. The poleward wind intensification at the polar cap caused by substorm energy injection can be seen in the numerical simulation by FUJIWARA *et al.* (1996). However, few investigations of such poleward winds have been carried out.

4.2. Periodic enhancements of meridional winds on the night of 3–4 June 1994

In this section, we will present an example of periodic enhancements of meridional wind velocities observed in the *F*- and *E*-regions on the night of 3–4 June 1994. In order to compare the pattern of meridional winds on the inner fringe with those on the outer fringe, we selected four locations, which were the southern part on the outer fringe (S_out) and inner fringe (S_in), and the northern part on the outer fringe (N_out) and inner fringe (N_in). Figures 6 and 7 show LOS wind velocities at the four locations for the *F*- and *E*-regions, respectively, on the night of 3–4 June 1994. These wind variations were observed during a geomagnetically active period with K_p values ranging from 3 to 5 (see Fig. 2). On this night, wind velocities were derived every ~5 min, but obtained data were smoothed by the boxcar average of a 5-point width. The hatched areas between 2300 UT and 0400 UT in Figs. 6 and 7 indicate periodic enhancements of poleward winds in the *F*- and *E*-regions, respectively, and the solid lines connecting the peaks indicate that the variations propagate from north to south (poleward). The periods of the variations were 1.3–2 hr (*F*-region) and 1.2 hr (*E*-region), while the speeds of poleward propagation were ~80 m/s (*F*-region) and ~110 m/s (*E*-region). These parameters in the *F*- and *E*-regions were similar to one another. They may be

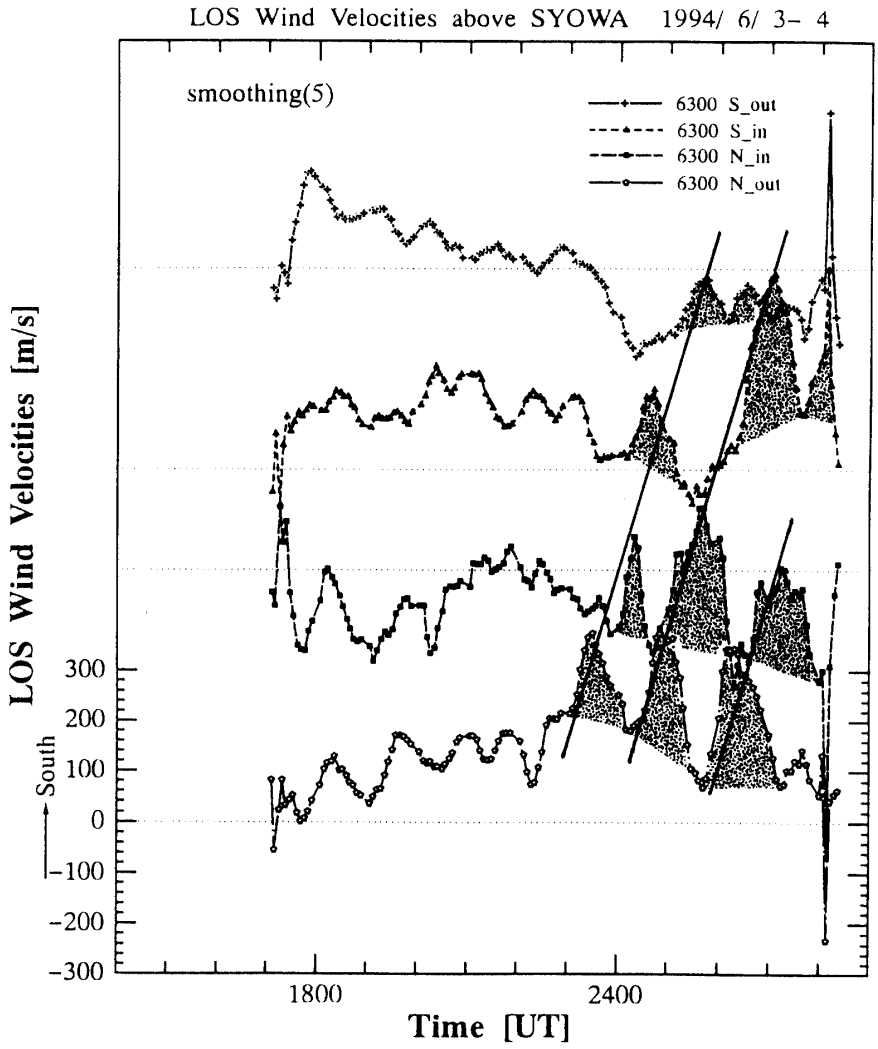

Fig. 6. Variations in LOS wind velocities at four points located along the geomagnetic meridian, for OI 630.0 nm emission on the night of 3–4 June 1994.

middle-scale atmospheric gravity waves (AGWs) with a commonly accepted size classification nomenclature (FRANCIS, 1975; RICHMOND and ROBLE, 1979; HUNSUCKER, 1982). Auroral energy appears to be important as a possible source for middle-scale AGWs. Figure 8 shows relative variations in OI 630.0 nm emission intensities on this night at the four locations. Before midnight, there was auroral activity above Syowa Station. However, when the periodic enhancements of poleward winds were observed between 2300 UT and 0300 UT, there was no auroral activity within a few hundred kilometers from Syowa Station. At this time, Syowa Station was located on the poleward side of the auroral oval, and there was auroral activity a few hundred kilometers north of Syowa Station.

In a recent study, similar phenomena were reported by FAGUNDES *et al.* (1995). They measured the OI 630.0 nm emission line intensity profile and meridional wind velocities at Kiruna using an imaging Fabry-Perot interferometer, and determined the location of auroral electrojets from magnetic field measurement. Their observational

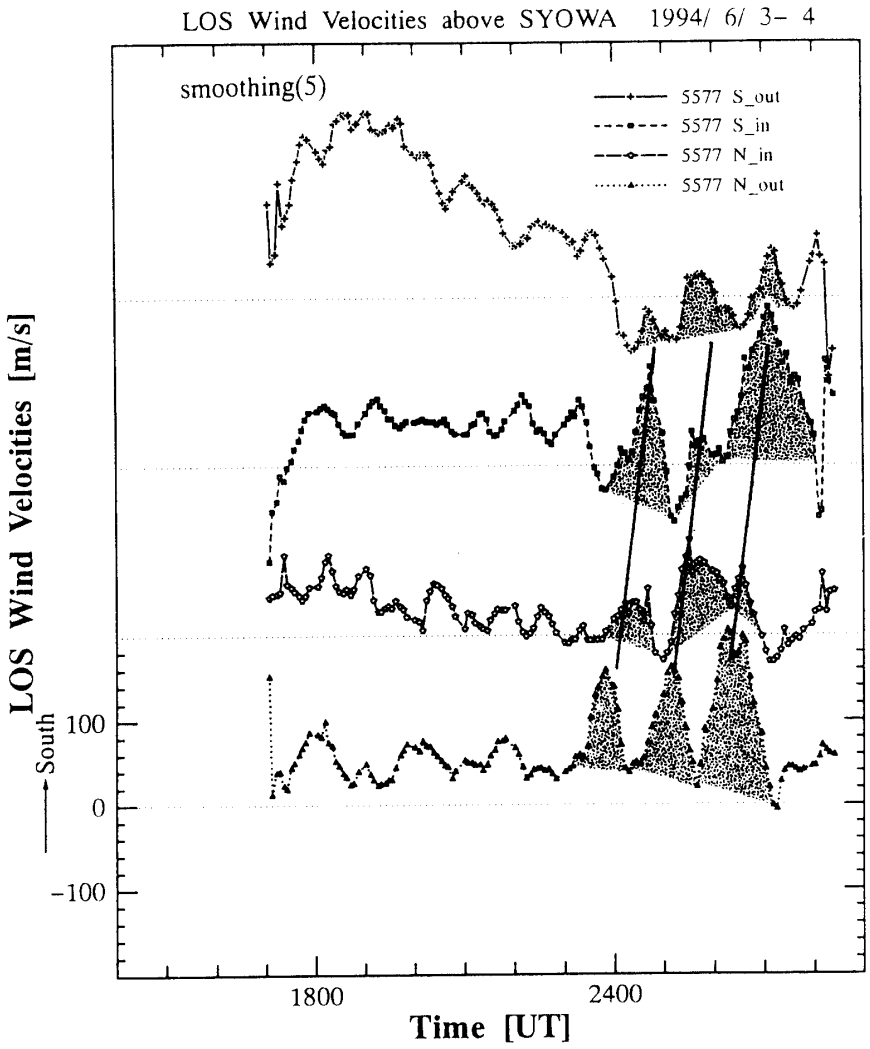

Fig. 7. Same as Fig. 6 except for the OI 557.7 nm emission.

results indicated that a large perturbation in the thermospheric winds was generated when the OI 630.0 nm line intensity showed an enhancement and/or auroral electrojets were close to, or over, the Kiruna latitude. These phenomena were thought to be due to large-scale atmospheric gravity waves. The gravity waves observed were propagating equatorward with speeds of 890 m/s and 530 m/s or northward with a speed of 380 m/s.

In Figs. 6 and 7, we find many complex variations in winds besides the periodic enhancements mentioned above. This suggests that various kinds of waves are generated in the auroral oval. Most of these seem to dissipate then and there, and only a few variations propagate toward different places. It is known that AGWs are an essential auroral energy transfer process in the high-latitude thermosphere. To investigate the generation and propagation mechanisms of AGWs in detail, simultaneous observations at several points along a meridian separated by several hundred kilometers would be effective.

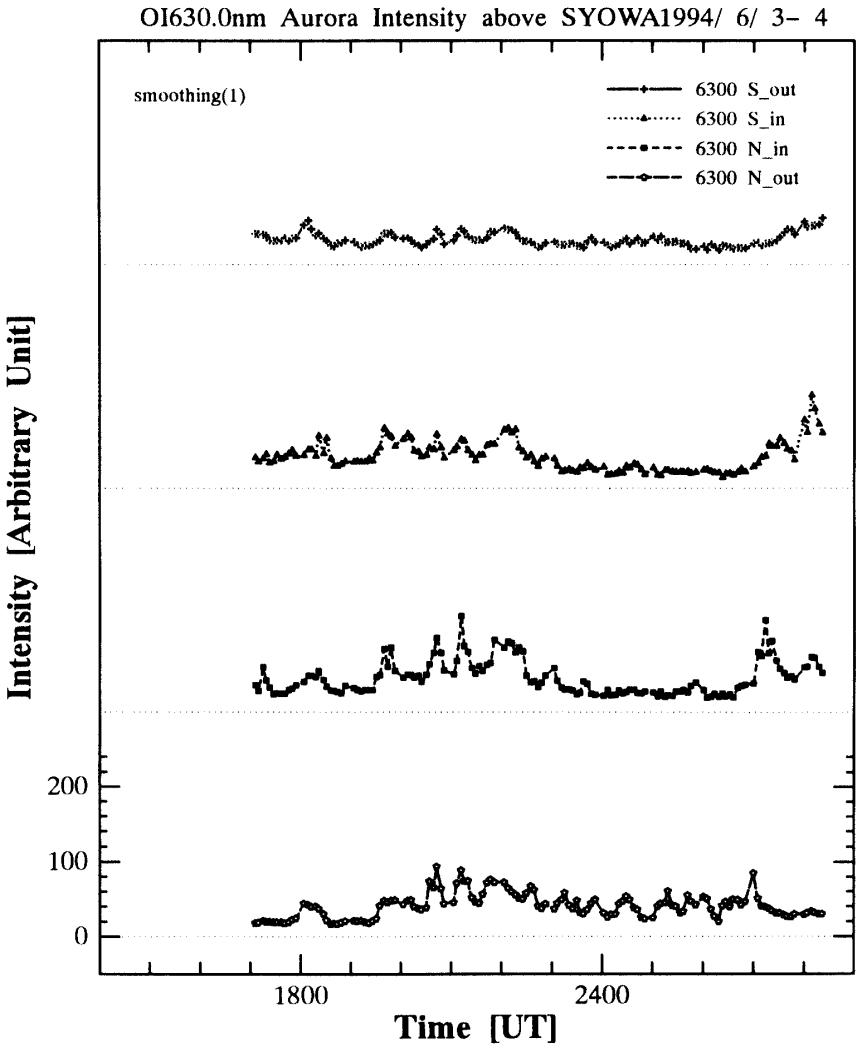

Fig. 8. Variations in the OI630.0 nm emission intensities at four points located along the geomagnetic meridian, for the night of 3–4 June 1994.

5. Conclusions

The conclusions of this paper are summarized as follows:

1) Nighttime variations in the thermospheric neutral winds were found to depend on geomagnetic activity. Magnetic southward winds during geomagnetically active periods are stronger than during quiet periods, and the difference in the wind velocities on active and quiet days is largest around midnight. The difference is supposed to be associated with the auroral energy injection level and the relative location between the auroral oval and Syowa Station.

2) Periodic enhancements of meridional wind velocities were observed in the *F*- and *E*-regions on the night of 3–4 June 1994. The periods of the variations were 1.3–2 hr in the *F*-region and 1.2 hr in the *E*-region, while the speeds of poleward propagation were ~80 m/s in the *F*-region and ~110 m/s in the *E*-regions. When these periodic enhancements appeared, Syowa Station was located on the poleward side of the auroral oval, and

there was auroral activity at a distance of a few hundred kilometers north of Syowa Station. These may have been middle-scale atmospheric gravity waves (AGWs) conforming to a commonly accepted size classification nomenclature.

These observational results demonstrated that the FPDIS is an outstanding tool for the remote sensing of rapid variations in the thermospheric neutral winds associated with auroral activity, and they demonstrated several types of thermospheric responses to auroral activity.

To investigate the generation and propagation mechanisms of AGWs in detail, it will be effective to carry out simultaneous observations at several points along a meridian separated by several hundred kilometers. Further, simultaneous observations of thermosphere and ionosphere by the FPDIS and various kinds of radars would be useful for a clearer and more comprehensive understanding of the thermosphere.

References

ARMSTRONG, E.B. (1969): Doppler shifts in the wavelength of the OI λ6300 line in the night airglow. Planet. Space Sci., **17**, 957–974.

BATTEN, S., REES, D., WADE, D. and STEEN, A. (1988): Observations of thermospheric neutral winds by the UCL Doppler imaging system at Kiruna in northern Scandinavia. J. Atmos. Terr. Phys., **50**, 861–888.

BATTEN, S. and REES, D. (1990): Thermospheric winds in the auroral oval: Observations of small scale structures and rapid fluctuations by a Doppler imaging system. Planet. Space Sci., **38**, 675–694.

BURNSIDE, R.G., HERRERO, F.A., MERIWETHER. J.W., Jr. and WALKER, J.C.G. (1981): Optical observations of thermospheric dynamics at Arecibo. J. Geophys. Res., **86**, 5532–5540.

FAGUNDES, P.R., ARULIAH, A.L., REES, D. and BITTENCOURT, J.A. (1995): Gravity wave generation and propagation during geomagnetic storms over Kiruna (67.8°N, 20.4°E). Ann. Geophys., **13**, 13358–13366.

FELDSTEIN , Y.I. and STARKOV, G.V. (1967): Dynamics of auroral belt and polar geomagnetic disturbances. Planet. Space Sci., **15**, 209–229.

FOSTER, J.C., ST.-MAURICE, J.-P. and ABREU, V.J. (1983): Joule heating at high latitudes. J. Geophys. Res., **88**, 4885–4897.

FRANCIS, S.H. (1975): Global propagation of atmospheric gravity waves: a review. J. Atmos. Terr. Phys., **37**, 1011–1054.

FUJIWARA, H., MAEDA, S., FUKUNISHI, H., FULLER-ROWELL, T.J. and EVANS, D.S. (1996): Global variations of thermospheric winds and temperatures caused by substorm energy injection. J. Geophys. Res., **101**, 225–239.

HAYS, P.B. and ROBLE, R.G. (1971): Direct observations of thermospheric winds during geomagnetic storms. J. Geophys. Res., **76**, 5316–5321.

HAYS, P.B., MERIWETHER, J.W. and ROBLE, R.G. (1979): Nighttime thermospheric winds at high latitudes. J. Geophys. Res., **84**, 1905–1913.

HERNANDEZ, G. and ROBLE, R.G. (1976): Direct measurement of nighttime thermospheric winds and temperatures. 1. Seasonal variations during geomagnetic quiet periods. J. Geophys. Res., **81**, 2065–2074.

HERNANDEZ, G., SMITH, R.W., ROBLE, R.G., GRESS, J. and CLARK, K.C. (1990): Thermospheric dynamics at the south pole. Geophys. Res. Lett., **17**, 1255–1258.

HUNSUCKER, R.D. (1982): Atmospheric gravity waves generated in the high-latitude ionosphere: A review. Rev. Geophys., **20**, 293–315.

JACKA, F., BOWER, A.R.D. and WILKSCH, P.A. (1979): Thermospheric temperatures and winds derived from OI λ630 nm night airglow line profiles. J. Atmos. Terr. Phys., **41**, 397–407.

KUBOTA, M. (1996): A study on middle-scale variations of thermospheric neutral winds associated with auroral activity over Syowa Station, Antarctica. Doctor Thesis, Tohoku University, Japan, 143 p.

MERIWETHER, J.W., Jr., KILLEEN, T.L., MCCORMAC, F.G., Burns, A.G. and ROBLE, R.G. (1988): Thermospheric winds in the geomagnetic polar cap for solar minimum conditions. J. Geophys. Res., **93**, 7478–7492.

NAKAJIMA, H. (1993): A study on auroral zone thermospheric neutral temperatures and winds using Fabry-Perot Doppler imaging observations at Syowa Station, Antarctica. Doctor Thesis, Tohoku University, Japan, 176 p.

NAKAJIMA, H., OKANO, S., FUKUNISHI, H. and ONO, T. (1995): Observations of thermospheric wind velocities and temperatures by the use of a Fabry-Perot Doppler imaging system at Syowa Station, Antarctica. Appl. Opt., **34**, 8382–8395.

REES, D. and GREENAWAY, A.H. (1983): Doppler imaging system; an optical device for measuring vector winds. 1: General principles. Appl. Opt., **22**, 1078–1083.

REES, D., SMITH, R.W., CHARLETON, P.J., MCCORMAC, F.G. and STEEN, A. (1984): The generation of vertical thermospheric winds and gravity waves at auroral latitudes-I. Observations of vertical winds. Planet. Space Sci., **32**, 667–684.

REES, M.H., EMERY, B.A., ROBLE, R.G. and STAMNES, K. (1983): Neutral and ion gas heating by auroral particle precipitation. J. Geophys. Res., **88**, 6289–6300.

RICHMOND, A.D. and ROBLE, R.G. (1979): Dynamic effects of aurora generated gravity waves on the mid-latiude ionosphere. J. Atmos. Terr. Phys., **41**, 841–852.

ROBLE, R.G. and RIDLEY, E.C. (1987): An auroral model for the NCAR thermospheric general circulation model (TGCM). Ann. Géophys., **5A**, 369–382.

SICA, R.J., HERNANDEZ, G., EMERY, B.A., ROBLE, R.G., SMITH, R.W. and REES, M.H. (1989): The control of auroral zone dynamics and thermodynamics by the interplanetary magnetic fields dawn-dusk (Y) component. J. Geophys. Res., **94**, 11921–11932.

SIPLER, D.P. and BIONDI, M.A. (1979): Midlatitude *F* region neutral winds and temperatures during the geomagnetic storm of March 26, 1976. J. Geophys. Res., **84**, 37–40.

(Received June 6, 1997; Revised manuscript accepted Novemver 10, 1997)